

DETC2022-90726

LEVEL-SET-BASED SHAPE & TOPOLOGY OPTIMIZATION OF THERMAL CLOAKS

Xiaoqiang Xu

Department of Mechanical Engineering
State University of New York at Stony Brook
Stony Brook, NY 11794, USA
Email: xiaoqiang.xu@stonybrook.edu

Shikui Chen*

Department of Mechanical Engineering
State University of New York at Stony Brook
Stony Brook, NY 11794, USA
Email: shikui.chen@stonybrook.edu

ABSTRACT

Thermal metamaterials are gaining increasing popularity, especially for heat flux manipulation purposes. However, due to the high anisotropy of the structures resulting from the transformation thermotics or scattering cancellation methods, researchers are resorting to topology optimization as an alternative to find the optimal distribution of constituent bulk materials to realize a specific thermal function. This paper proposes to design a thermal cloak using the level-set-based shape and topology optimization. The thermal cloak design is considered in the context of pure heat conduction. The cloaking effect is achieved by reproducing the reference temperature field through the optimal distribution of two thermally conductive materials. The structural boundary is evolved by solving the Hamilton-Jacobi equation. The feasibility and validity of the proposed method to design thermal meta-devices with cloaking functionality are demonstrated through two numerical examples. The optimized structures have clear boundaries between constituent materials and do not exhibit thermal anisotropy, making it easier for physical realization. The first example deals with a circular cloaking region as a benchmark design. The robustness of the proposed method against various cloaking regions is illustrated by the second example concerning a human-shaped cloaking area. This work can inspire a broader exploration of the thermal meta-device in the heat flux manipulation regime.

Keywords

Thermal cloak. Heat flux manipulation. Topology optimization. Level set method.

1 INTRODUCTION

Thermal metamaterials with elegantly engineered structures have undergone considerable development in recent years [1–3]. One important function of such thermal metamaterials is manipulating the heat flux as desired. To this end, a number of thermal metamaterial devices have been designed and even physically realized, e.g., thermal cloak [4,5], thermal concentrator [6,7], thermal rotator [8–10] and thermal camouflage [11]. Thermal metamaterial design are the scattering cancellation method [5,12] and the transformation thermotics method [3,13], inspired and developed from the pioneering transformation optics [14,15]. The basic idea behind transformation thermotics is that to maintain the invariance of the domain equation under coordinate transformation, the related physics property, i.e., thermal conductivity tensor, must be properly modified. As a result, the thermal metamaterials obtained through transformation thermotics often exhibit high anisotropy and inhomogeneity, posing a great challenge for physical realization. A common treatment is to employ a multi-layered structure [10,16], but often at the expense of some loss of accuracy. We briefly mention some of the previous research endeavors using the methods mentioned above. Imran et al. [16] and Dede et al. [17] explored the heat flow control devices considering the convection effect. Vemuri et al. [18] managed to guide the conductive heat flux by properly position-

*Address all correspondence to this author.

ing and orienting the nominally isotropic material. Moccia et al. [19] realized the independent manipulation of heat and electrical current, pushing one step further toward the “transformation multiphysics”. An intelligent thermal metamaterial was developed in [7], which exhibits either cloaking or concentrating functionality depending on the ambient temperature.

There have also been efforts to design thermal metamaterials using natural materials to avoid high anisotropy. For example, a thermal camouflage device was demonstrated in [20], which was directly derived from the conduction equation and could produce a different thermal scattering signature than expected. The research studies in [5, 12, 21] focused on experimental validation of thermal meta-devices with various functionalities.

Recently, numerical optimization has been integrated into thermal metamaterial designs. Dede et al. [22] examined the thermal-composite design for heat flux shielding, focusing, and reversal by optimizing the inclusion angles in a surrounding medium. Peralta et al. [23] employed the density-based optimization method to design a thermal concentrator without disturbing the external reference temperature field. Subsequent work from Peralta et al. [24] focused on the fabricability of the heat flux manipulation devices. A number of papers [4, 6, 25] dealt with the topology optimization of thermal meta-devices with a level set representation using the covariance matrix adaptation evolution strategy (CMA-ES) to search for the optimal designs. Seo et al. [26] proposed a multi-scale topology optimization method using only a single variable for heat flux control purposes. The multi-scale method was shown to be more advantageous over the various composition ratios of the highly conductive material than the single-scale counterpart. Yet, the optimized designs did not have quite crisp boundaries. Sha et al. [11] came up with an illusion device using the density-based topology optimization, where the heat source is camouflaged while keeping the exterior temperature field unaltered. A recent work from Sha et al. [8] combined the transformation thermotics and topology optimization to successfully design thermal meta-devices with omnidirectional thermal functionalities.

In this study, we try to contribute by designing a thermal cloak using the level-set-based topology optimization. The objection function will be the least square error of the temperature field from the current design with a predefined reference temperature field in a specific evaluation domain. Two bulk materials with distinct thermal conductivity, i.e., iron and aluminum, will be properly distributed in the design domain to minimize the temperature perturbation in the evaluation domain. The clear boundaries between different material phases make it easy to generate 3D models and conduct physical experiments. The optimized iron/aluminum configuration exhibits the thermal cloaking functionality. The robustness of the proposed method against different cloaking region shapes is demonstrated by considering a human-shaped cloaking area.

This paper is organized as follows: Section 2 will provide

the problem formulation and shape sensitivity analysis. Numerical examples including two designs will be presented in Section 3. Section 4 will contain some discussions with closing remarks.

2 SHAPE AND TOPOLOGY OPTIMIZATION OF THERMAL CLOAKS

2.1 Problem Formulation

This paper is interested in designing thermal cloaks using level-set-based topology optimization. For simplicity, we consider a 2D steady-state heat conduction problem. All related physical properties are assumed to be isotropic. The governing equations for pure heat conduction phenomena are given as follows:

$$\begin{aligned} -k\nabla^2 T &= 0, \text{ in } \Omega \\ k\nabla T \cdot \mathbf{n} &= 0, \text{ on } \Gamma_H \\ T &= T_h, \text{ on } \Gamma_{D1} \\ T &= T_l, \text{ on } \Gamma_{D2} \end{aligned} \quad (1)$$

where k is the thermal conductivity, T is the state variable temperature, \mathbf{n} is the outward unit vector of the structural boundary. There is no body heat source term, nor is there boundary heat flux. As shown in Figure 1, the whole computational model consists of the insulator domain Ω_{ins} , the design domain Ω_D and the outer domain Ω_{out} . Two Dirichlet boundary conditions are applied with $T_h = 10K$ and $T_l = 0K$. All other boundaries are adiabatic. Ω_{ins} is the region of interest that we want to cloak. By cloaking, it means that there should be no temperature gradient inside Ω_{ins} . Suppose we simply dig the insulator domain Ω_{ins} out of a reference domain, which is solely filled with single material iron. In that case, it will cause some disturbance on the temperature distribution on Ω_{out} . Suppose a thermal sensor is employed to evaluate the temperature perturbation in Ω_{out} , it would detect the existence of the insulator region, i.e., it is not clocked. It then becomes reasonable to introduce some aluminum with higher thermal conductivity to compensate for the extremely low thermal conductivity brought by the insulator region Ω_{in} . An optimal distribution between iron and aluminum in the design domain Ω_D can be sought after by topology optimization. Ω_{out} will be fixed with iron.

The objective of the optimization is to minimize the least square error between the temperature fields in the exterior domain Ω_{out} . The formal optimization problem is formulated as follows:

$$\begin{aligned} \text{Inf}_{\Phi} J &= \frac{1}{J_n} \int_{\Omega_{out}} |T - T_{ref}|^2 d\Omega, \\ \text{s.t. } a(T, \bar{T}) &= 0, \forall \bar{T} \in U_{ad} \end{aligned} \quad (2)$$

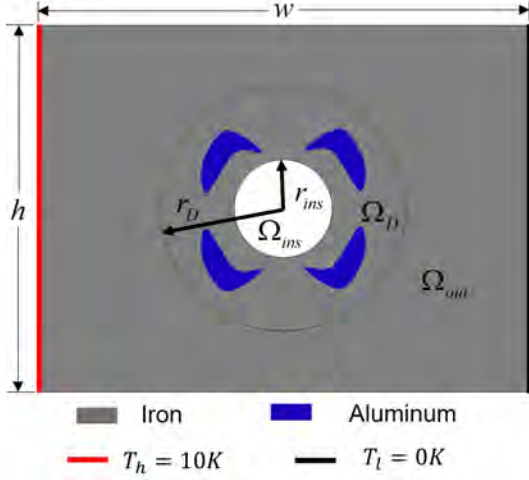


FIGURE 1. THE DIAGRAM OF A THERMAL CLOAK WITH A CIRCULAR INSULATOR. $w = 4m, h = 3m, r_{ins} = 0.4m, r_D = 1m$. $k_{aluminum} = 204W/(m \cdot K), k_{iron} = 67W/(m \cdot K)$.

where $a(T, \bar{T}) = \int_{\Omega} k \nabla T \cdot \nabla \bar{T} d\Omega$. \bar{T} is the test function and U_{ad} is the space of the virtual temperature field satisfying the same boundary conditions. T_{ref} is the reference temperature field when all the domains are occupied by iron. J_n is a constant normalization term to keep the objective value in a moderate range. J_n is given as:

$$J_n = \int_{\Omega_{out}} |T_0 - T_{ref}|^2 d\Omega, \quad (3)$$

where T_0 is the temperature field when the design domain Ω_D is filled with only iron. The Φ refers to the level set function.

Initiated by Sethian and Wiegmann [27] and further completed by Wang [28] and Allaire [29] respectively, the level set method has become a promising shape and topology optimization approach. A clear boundary between different phases can be generated and maintained during the optimization process, which is a much desired property when a detailed description of the boundary is required. The structural boundary is implicitly represented as the zero contour of a one-higher dimensional level set function. The level set function is defined on a fixed background grid in the classical level set framework. The structural design is implicitly embedded in the level set function $\Phi(\mathbf{x}, t)$ as follows:

$$\begin{cases} \Phi(\mathbf{x}, t) > 0, & x \in \Omega, & \text{material} \\ \Phi(\mathbf{x}, t) = 0, & x \in \partial\Omega, & \text{boundary} \\ \Phi(\mathbf{x}, t) < 0, & x \in D/\Omega, & \text{void} \end{cases} \quad (4)$$

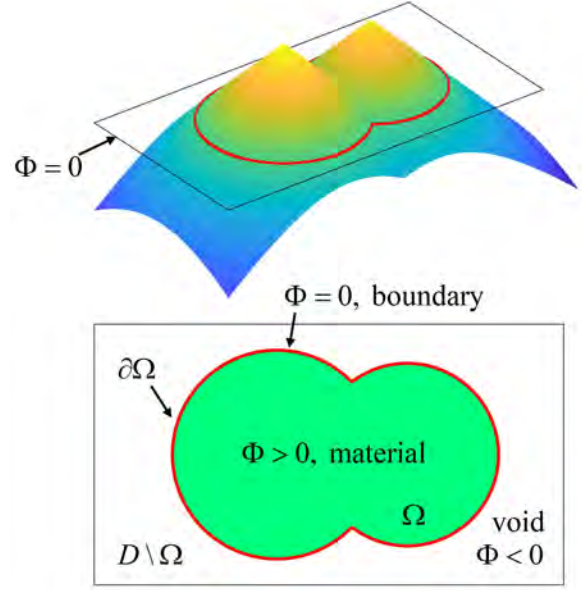


FIGURE 2. THE LEVEL SET REPRESENTATION OF A 2D DESIGN

The geometric level set model for a 2D structural boundary is shown in Figure 2. For the structural boundary, it always satisfies the equation $\Phi(\mathbf{x}, t) = 0$. By differentiating both sides of the equation with respect to a pseudo time t , we could obtain the Hamilton-Jacobi (H-J) equation [30]:

$$\frac{\partial \Phi(\mathbf{x}, t)}{\partial t} - V_n \cdot |\nabla \Phi| = 0, \quad (5)$$

where $V_n = V \cdot \left(-\frac{\nabla \Phi}{|\nabla \Phi|}\right) = \frac{dx}{dt} \cdot \left(-\frac{\nabla \Phi}{|\nabla \Phi|}\right)$. By solving the above H-J equation iteratively, the level set function is updated to drive the evolution of the structural boundary. The normal velocity V_n can be obtained from shape sensitivity analysis, which is usually derived using the adjoint method.

In this study, the level set function Φ is defined on the design domain Ω_D . Specifically, $\Phi > 0$ refers to the aluminum domain Ω_{alum} and $\Phi < 0$ represents the iron domain Ω_{iron} . The structural boundary between aluminum and iron is given as $\Phi = 0$. There is no void phase in the design domain Ω_D . We follow the problem setting proposed by Fujii et al. [4].

2.2 Shape Sensitivity Analysis

As can be seen from equation (5), the normal velocity V_n is needed to solve the H-J equation. V_n can be obtained from shape sensitivity analysis [28, 29]. In this study, we employ the material derivative method [31] and adjoint method [32] to derive the shape derivative.

The Lagrangian of the optimization problem is defined as

$$L = J(T) + a(T, \bar{T}). \quad (6)$$

The material derivative of the Lagrangian is given:

$$\frac{DL}{Dt} = \frac{DJ(T)}{Dt} + \frac{Da(T, \bar{T})}{Dt}. \quad (7)$$

In this problem formulation, the objective function is evaluated on Ω_{out} , which is different from the design domain Ω_D . We rewrite the objective function J as follows:

$$J = \frac{1}{J_n} \int_{\Omega_{out}} |T - T_{ref}|^2 d\Omega = \frac{1}{J_n} \int_{\Omega} g(x) \cdot |T - T_{ref}|^2 d\Omega, \quad (8)$$

where $g(x)$ is a window function, which takes value 1 in domain Ω_{out} , and 0 in domain Ω_D and Ω_{ins} .

The material derivative of the objective function $J(T)$ is:

$$\begin{aligned} \frac{DJ(T)}{Dt} &= \frac{1}{J_n} \int_{\Omega} 2g(x) \cdot (T - T_{ref}) \cdot T' d\Omega \\ &+ \frac{1}{J_n} \int_{\partial\Omega} g(x) \cdot |T - T_{ref}|^2 \cdot V_n ds. \end{aligned} \quad (9)$$

The material derivative of the weak-form governing equation is:

$$\begin{aligned} \frac{Da(T, \bar{T})}{Dt} &= \int_{\Omega} k[\nabla T' \cdot \nabla \bar{T} + \nabla T \cdot \nabla \bar{T}'] d\Omega \\ &+ \int_{\partial\Omega} k\nabla T \cdot \nabla \bar{T} \cdot V_n ds. \end{aligned} \quad (10)$$

Collecting all the terms containing \bar{T}' as follows:

$$\int_{\Omega} k\nabla T \cdot \nabla \bar{T}' d\Omega = 0. \quad (11)$$

we recover the weak form of the state equation as $a(T, \bar{T}') = 0$, for $\forall \bar{T}' \in U_{ad}$. Collecting the terms containing T' and making the sum equal to zero, we can obtain the adjoint equation:

$$\frac{1}{J_n} \int_{\Omega} 2g(x) \cdot (T - T_{ref}) \cdot T' d\Omega + \int_{\Omega} k\nabla T' \cdot \nabla \bar{T} d\Omega = 0. \quad (12)$$

The above adjoint equation (12) is solved for \bar{T} . The remaining part for the material derivatives of the Lagrangian L reads:

$$\frac{DL}{Dt} = \frac{1}{J_n} \int_{\partial\Omega} g(x) \cdot |T - T_{ref}|^2 \cdot V_n ds + \int_{\partial\Omega} k\nabla T \cdot \nabla \bar{T} \cdot V_n ds \quad (13)$$

Applying the steepest descent method, the design velocity field can be constructed as:

$$V_n = -\frac{1}{J_n} g(x) \cdot |T - T_{ref}|^2 - k\nabla T \cdot \nabla \bar{T}. \quad (14)$$

3 NUMERICAL EXAMPLES

3.1 A Thermal Cloak With Circular Insulator

For better visualization effect to display the temperature field comparisons, the temperature field is normalized in this way: $T_i^n = (T_i - T_l)/(T_h - T_l)$, where $T_i = T, T_0$ or T_{ref} . As shown in Figure 3(a), a temperature field T_{ref} with uniform gradient is generated by filling Ω_D and Ω_{ins} with iron. When the insulator is presented in Ω_{ins} shown in Figure 3(b), the reference temperature field in Ω_{out} is obviously disturbed with nonparallel temperature contour lines. To alleviate this temperature perturbation and achieve the thermal cloak function, the iron and aluminum are optimally distributed in the design domain Ω_D using the level-set-based topology optimization algorithm.

The optimization result is shown in Figure 4. The ersatz material model is employed in the topology optimization formulation. Specifically, the central cloaked region, which is treated as the insulator, is also included in the finite element analysis but with a very tiny thermal conductivity $K_{ins} = 1 \times 10^{-5} W/(m \cdot K)$. The whole reference domain Ω (union of Ω_{ins} , Ω_D , and Ω_{out}) is

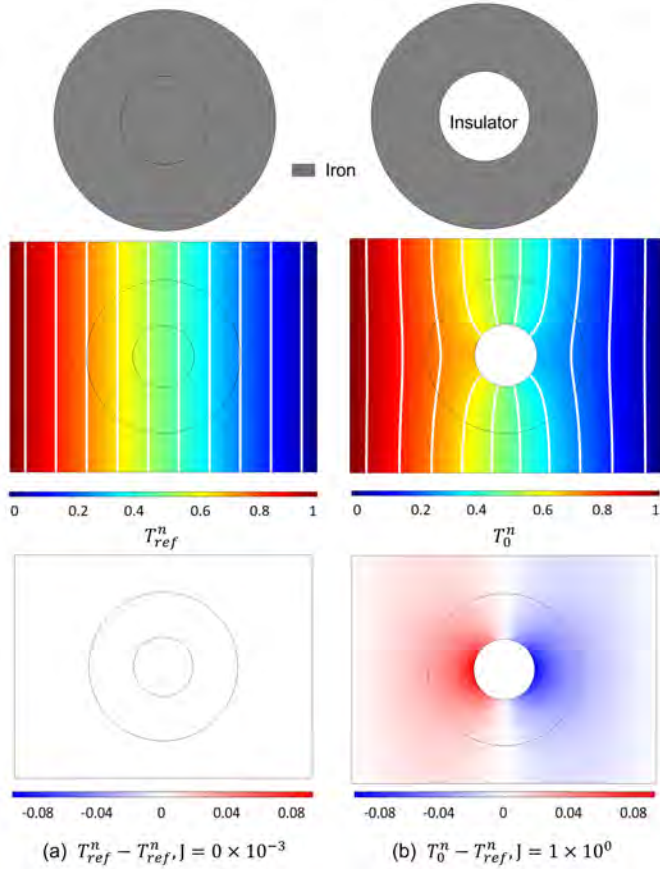


FIGURE 3. (a) Ω_D AND Ω_{ins} BOTH FILLED WITH IRON FOR T_{ref} TEMPERATURE FIELD, (b) Ω_D FILLED WITH IRON, AND Ω_{ins} WITH INSULATOR FOR T_0 TEMPERATURE FIELD.

meshed with uniform triangulation as shown in Figure 5. The total element number is 21916. The normalized temperature field T_n and the discrepancy with the normalized reference temperature field T_{ref}^n are displayed in Figure 6. The temperature contour lines in Ω_{out} region are almost parallel as they are when there is no insulator presented. The temperature difference in Ω_{out} is close to zero and negligible. The objective function $J = 1.53 \times 10^{-4}$, which is small enough to indicate that the insulator is effectively cloaked from being detected by evaluating the temperature field perturbation in Ω_{out} . It is worth noting that this optimized configuration is totally different from the result in [4], although they share similar problem formulation. This phenomenon is not uncommon in the optimization field. Normally, a local optimum will be found for most optimization problems if it is not a strictly convex problem. Several factors can affect the obtained local optimum, e.g., the initial guess and the optimization algorithm.

The convergence history plot for the thermal cloak with a circular insulator is given in Figure 7. There is no volume con-

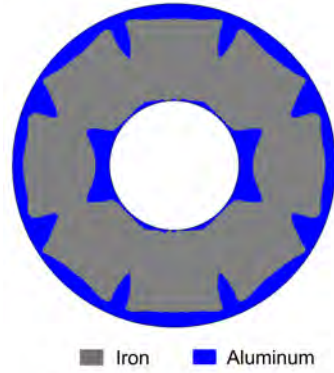


FIGURE 4. OPTIMIZATION RESULT FOR THE THERMAL CLOAK WITH CIRCULAR INSULATOR

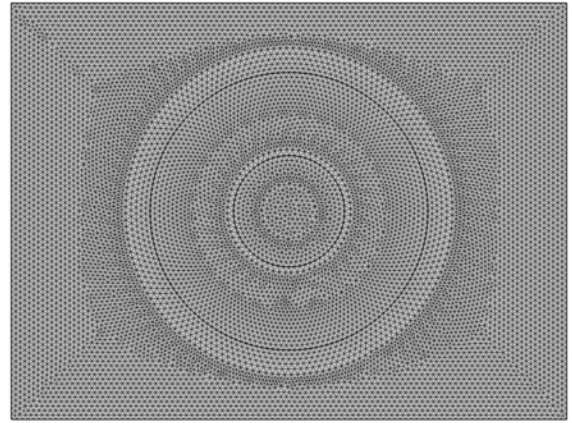


FIGURE 5. THE FINITE ELEMENT MESH FOR THE CIRCULAR CLOAK EXAMPLE

straint imposed on either the iron or the aluminum in this optimization. The aluminum accounts for 28.14% of the whole design domain area in Ω_D for the final optimal configuration.

3.2 Thermal Cloak With A Human-Shaped Insulator

The second numerical example deals with a similar problem-setting with a human-shaped insulator. The optimized structure is exhibited in Figure 8. The whole reference domain Ω (union of Ω_{ins} , Ω_D , and Ω_{out}) is meshed with triangulation. The total element number is 32798. Again, the temperature field in Ω_{out} with uniform gradient is reproduced as shown in Figure 9 (left). The temperature discrepancy between T^n with the normalized reference temperature field T_{ref}^n in Ω_{ins} is small enough to be neglected. The objective function $J = 9.26 \times 10^{-6}$.

The convergence history plot for the thermal cloak with a human-shaped insulator is shown in Figure 10. In the final op-

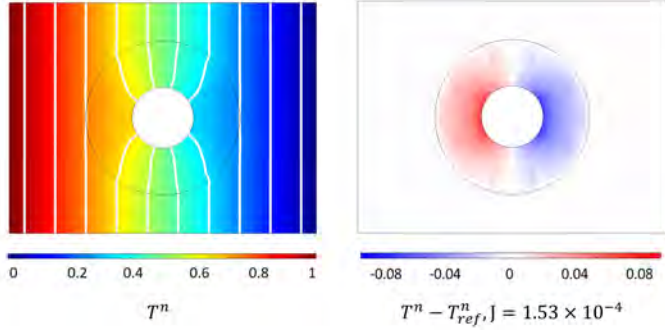


FIGURE 6. (EXAMPLE 3.1) LEFT: THE NORMALIZED TEMPERATURE FIELD T^n . RIGHT: THE DIFFERENCE WITH NORMALIZED REFERENCE FIELD T_{ref}^n

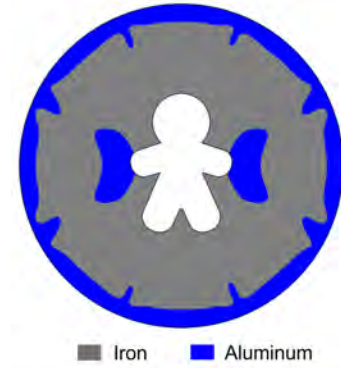


FIGURE 8. OPTIMIZATION RESULT FOR THE THERMAL CLOAK WITH HUMAN-SHAPED INSULATOR

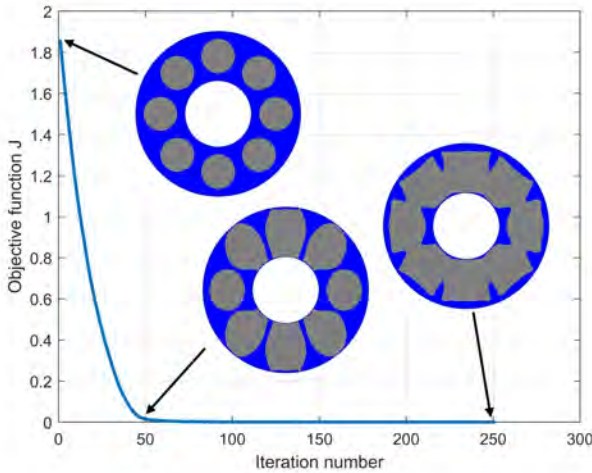


FIGURE 7. CONVERGENCE HISTORY FOR THE THERMAL CLOAK WITH CIRCULAR INSULATOR

timized configuration, 29.29% of Ω are occupied by aluminum. A clear boundary between the iron and aluminum is maintained during the optimization process. As a result, little post processing is needed to convert this structure into 3D printable models as shown in Figure 11.

4 DISCUSSIONS AND CONCLUSIONS

In this study, a level-set-based shape and topology optimization is proposed to design a thermal cloak by distributing two naturally occurring bulk thermal conduction materials, iron and aluminum, to eliminate the temperature disturbance on the evaluation domain caused by the insulator (cloaking region). The optimized structures exhibit the expected cloaking functionality, despite having simple shape and topology. Compared with the transformation thermotics or scattering cancellation methods,

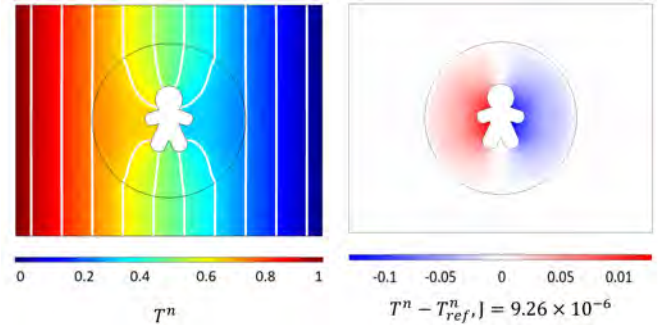


FIGURE 9. (EXAMPLE 3.2) LEFT: THE NORMALIZED TEMPERATURE FIELD T_n . RIGHT: THE DIFFERENCE WITH NORMALIZED REFERENCE FIELD T_{ref}^n

the proposed optimization algorithm is advantageous in that the resulting configuration does not possess any anisotropy, which could greatly facilitate the physical realization to further validate the cloaking performance.

Two numerical examples are considered in this paper. The first one serves as the benchmark example to draw some comparisons with literature results. It is worth mentioning that the optimized structure with a circular insulator has never been seen in the literature, yet it still renders a good cloaking performance. The second example deals with a thermal cloak with a human-shaped insulator. To the best of my knowledge, few research works have investigated the cloaking of an arbitrary shape. Most of the models considered are canonical shapes, e.g., circular and spherical. The second designed cloak with a human-shaped insulator will trigger more interest in the thermal cloak design for a broader application.

However, there are still some aspects that could be improved in the future. First, the optimized designs should be numerically verified and experimentally validated to make them more convincing. Second, the current designs are based on 2D planar ge-

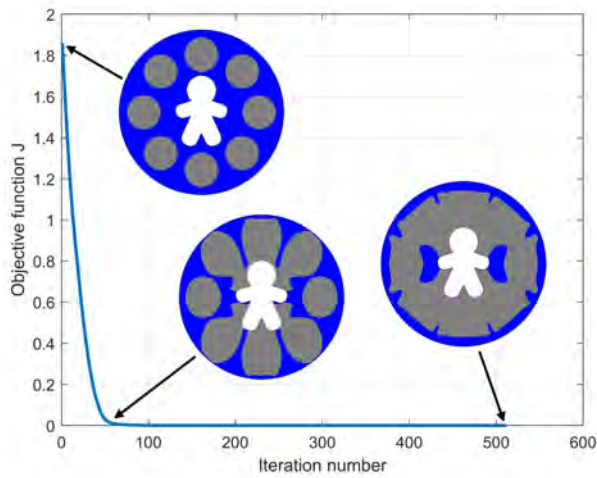


FIGURE 10. CONVERGENCE HISTORY FOR THE THERMAL CLOAK WITH HUMAN-SHAPED INSULATOR

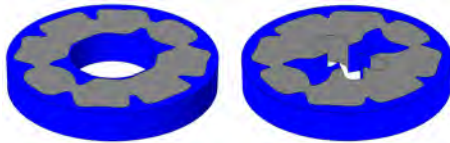


FIGURE 11. 3D CAD MODELS FOR THE OPTIMIZED CLOAKS WITH LEFT: CIRCULAR INSULATOR, RIGHT: HUMAN-SHAPED INSULATOR

ometry. In reality, the thermal cloak can take a free-form shape in 3D space. Designing a thermal cloak on the manifold will be our next research direction. Conformal mapping has been introduced into the level-set-based topology optimization community [33,34]. It shows great prospects in solving various optimization problems on free-form surfaces.

ACKNOWLEDGMENT

The authors gratefully acknowledge financial support from the National Science Foundation (CMMI-1762287), the Ford University Research Program (URP) (Award No. 2017-9198R), and the State University of New York (SUNY) at Stony Brook.

REFERENCES

- [1] Huang, J.-P., 2020. *Theoretical Thermotics*. Springer.
- [2] Sklan, S. R., and Li, B., 2018. “Thermal metamaterials: functions and prospects”. *National Science Review*, **5**(2), pp. 138–141.
- [3] Wang, J., Dai, G., and Huang, J., 2020. “Thermal metamaterial: fundamental, application, and outlook”. *Iscience*, **23**(10), p. 101637.
- [4] Fujii, G., Akimoto, Y., and Takahashi, M., 2018. “Exploring optimal topology of thermal cloaks by cma-es”. *Applied Physics Letters*, **112**(6), p. 061108.
- [5] Xu, H., Shi, X., Gao, F., Sun, H., and Zhang, B., 2014. “Ultra-thin three-dimensional thermal cloak”. *Physical Review Letters*, **112**(5), p. 054301.
- [6] Fujii, G., and Akimoto, Y., 2020. “Cloaking a concentrator in thermal conduction via topology optimization”. *International Journal of Heat and Mass Transfer*, **159**, p. 120082.
- [7] Shen, X., Li, Y., Jiang, C., Ni, Y., and Huang, J., 2016. “Thermal cloak-concentrator”. *Applied Physics Letters*, **109**(3), p. 031907.
- [8] Sha, W., Xiao, M., Zhang, J., Ren, X., Zhu, Z., Zhang, Y., Xu, G., Li, H., Liu, X., Chen, X., et al., 2021. “Robustly printable freeform thermal metamaterials”. *Nature communications*, **12**(1), pp. 1–8.
- [9] Zhou, L., Huang, S., Wang, M., Hu, R., and Luo, X., 2019. “While rotating while cloaking”. *Physics Letters A*, **383**(8), pp. 759–763.
- [10] Narayana, S., and Sato, Y., 2012. “Heat flux manipulation with engineered thermal materials”. *Physical review letters*, **108**(21), p. 214303.
- [11] Sha, W., Zhao, Y., Gao, L., Xiao, M., and Hu, R., 2020. “Illusion thermotics with topology optimization”. *Journal of Applied Physics*, **128**(4), p. 045106.
- [12] Han, T., Bai, X., Gao, D., Thong, J. T., Li, B., and Qiu, C.-W., 2014. “Experimental demonstration of a bilayer thermal cloak”. *Physical review letters*, **112**(5), p. 054302.
- [13] Fan, C., Gao, Y., and Huang, J., 2008. “Shaped graded materials with an apparent negative thermal conductivity”. *Applied Physics Letters*, **92**(25), p. 251907.
- [14] Pendry, J. B., Schurig, D., and Smith, D. R., 2006. “Controlling electromagnetic fields”. *science*, **312**(5781), pp. 1780–1782.
- [15] Leonhardt, U., 2006. “Optical conformal mapping”. *science*, **312**(5781), pp. 1777–1780.
- [16] Imran, M., Zhang, L., and Gain, A. K., 2020. “Advanced thermal metamaterial design for temperature control at the cloaked region”. *Scientific Reports*, **10**(1), pp. 1–11.
- [17] Dede, E. M., Nomura, T., Schmalenberg, P., and Seung Lee, J., 2013. “Heat flux cloaking, focusing, and reversal in ultra-thin composites considering conduction-convection effects”. *Applied Physics Letters*, **103**(6), p. 063501.
- [18] Vemuri, K. P., Canbazoglu, F., and Bandaru, P. R., 2014. “Guiding conductive heat flux through thermal metamaterials”. *Applied Physics Letters*, **105**(19), p. 193904.
- [19] Moccia, M., Castaldi, G., Savo, S., Sato, Y., and Galdi, V., 2014. “Independent manipulation of heat and electrical current via bifunctional metamaterials”. *Physical Review X*, **4**(2), p. 021025.
- [20] Han, T., Bai, X., Thong, J. T., Li, B., and Qiu, C.-W., 2014. “Full control and manipulation of heat signatures: cloaking, camouflage and thermal metamaterials”. *Advanced Materials*, **26**(11), pp. 1731–1734.
- [21] Schittny, R., Kadic, M., Guenneau, S., and Wegener, M., 2013. “Experiments on transformation thermodynamics: molding the flow of heat”. *Physical review letters*, **110**(19), p. 195901.
- [22] Dede, E. M., Nomura, T., and Lee, J., 2014. “Thermal-composite design optimization for heat flux shielding, focusing, and reversal”. *Structural and Multidisciplinary Optimization*, **49**(1), pp. 59–68.
- [23] Peralta, I., Fachinotti, V. D., and Ciarbonetti, Á. A., 2017. “Optimization-based design of a heat flux concentrator”. *Scientific reports*, **7**(1), pp. 1–8.
- [24] Peralta, I., and Fachinotti, V. D., 2017. “Optimization-based design of heat flux manipulation devices with emphasis on fabricability”. *Scientific reports*, **7**(1), pp. 1–8.
- [25] Fujii, G., and Akimoto, Y., 2019. “Optimizing the structural topology of bifunctional invisible cloak manipulating heat flux and direct current”. *Applied physics letters*, **115**(17), p. 174101.
- [26] Seo, M., Park, H., and Min, S., 2020. “Heat flux manipulation by using a single-variable formulated multi-scale topology optimization method”. *International Communications in Heat and Mass Transfer*, **118**, p. 104873.
- [27] Sethian, J. A., and Wiegmann, A., 2000. “Structural boundary design via level set and immersed interface methods”. *Journal of computational physics*, **163**(2), pp. 489–528.
- [28] Wang, M. Y., Wang, X., and Guo, D., 2003. “A level set method for structural topology optimization”. *Computer methods in applied mechanics and engineering*, **192**(1-2), pp. 227–246.
- [29] Allaire, G., Jouve, F., and Toader, A.-M., 2004. “Structural optimization using sensitivity analysis and a level-set method”. *Journal of computational physics*, **194**(1), pp. 363–393.
- [30] Osher, S., Fedkiw, R., and Piechor, K., 2004. “Level set methods and dynamic implicit surfaces”. *Appl. Mech. Rev.*, **57**(3), pp. B15–B15.
- [31] Choi, K. K., and Kim, N.-H., 2004. *Structural sensitivity analysis and optimization 1: linear systems*. Springer Science & Business Media.
- [32] Allaire, G., 2015. “A review of adjoint methods for sensitivity analysis, uncertainty quantification and optimization in numerical codes”. *Ingénieurs de l’Automobile*, **836**,

pp. 33–36.

- [33] Ye, Q., Guo, Y., Chen, S., Lei, N., and Gu, X. D., 2019. “Topology optimization of conformal structures on manifolds using extended level set methods (x-lsm) and conformal geometry theory”. *Computer Methods in Applied Mechanics and Engineering*, **344**, pp. 164–185.
- [34] Xu, X., Chen, S., Gu, X. D., and Wang, M. Y., 2021. “Conformal topology optimization of heat conduction problems on manifolds using an extended level set method (x-lsm)”. In *International Design Engineering Technical Conferences and Computers and Information in Engineering Conference*, Vol. 85390, American Society of Mechanical Engineers, p. V03BT03A030.